Int. J. Solids Structures Vol. 16, pp. 959–968
Pergamon Press Ltd., 1980. Printed in Great Britain

ELASTIC STRESS ANALYSIS OF CONSTRAINED CYLINDERS BY A SPECIAL FINITE ELEMENT METHOD

J. S. SOLECKI and J. L. SWEDLOW
Department of Mechanical Engineering, Carnegie Institute of Technology, Carnegie-Mellon University, Pittsburgh, PA 15213, U.S.A.

(*Received* 26 *March* 1980)

Abstract—A method is given for computing the strength and intensity of stress singularities in cylindrical configurations. The method uses special finite elements that are formulated with a variable singularity strain matrix, in conjunction with a simple minimum potential energy technique. Four distinct combinations of geometry and loading are treated. Results are shown to have high resolution and are in good agreement with available theory.

INTRODUCTION

A recurring problem in elasticity involves a right circular cylinder under axial load but having constrained or clamped ends, as in Fig. 1. The key issue is characterization of the singularity in strain and stress at the "corner", i.e. along the intersection of the cylindrical surface and the planar end. The singularity arises because the cylindrical surface is traction-free, while a high level of shear is required to constrain the end against radial motion. There is then a discontinuity in the shear, just at the corner, and the remaining components of strain and stress become singular.

Studies of this problem date at least from 1902, with Filon's work[1]. Many other approaches have been taken, mainly within the last two decades[2–10]. Various methods have been employed, including Fourier analysis[2], variational techniques[3], collocation[4, 5], and eigenfunction expansions[6–10]; the quality of result—especially in terms of convergence—appears to reflect the technique used.

The most recent work[9, 10] attacks the presence of a singularity directly and has sought to determine both its character, i.e. strength and its intensity. Both analyses utilize a local toroidal coordinate system, (ρ, ϕ) in Fig. 1 and both replace the presence of the coordinate r by a binomial expansion in terms of the (ρ, ϕ) system. Then, following the template of Williams's formulation[11], boundary conditions at $\phi = 0$ and $\phi = \pi/2$ are imposed to delimit those solutions to the field equations acceptable for subsequent analysis. In both cases, an eigen-equation is derived, solutions to which lead to formulae for stress which may then be patched into the otherwise smooth solution for the bulk of the cylinder.

It is to be noted that the eigen-equations developed by Zak[9] and by Benthem and Minderhoud[10] are the same; the difference between these two efforts is largely the manner in

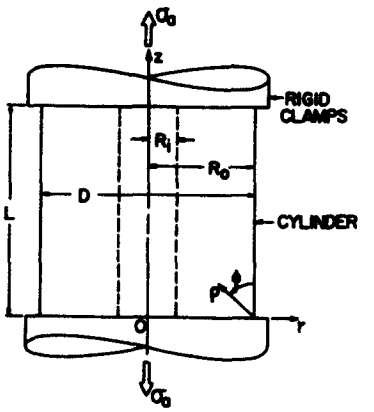

Fig. 1. A cylinder with constrained ends.

which the localized analysis is integrated with the global analysis. It is to be noted further that the eigen-equations derived in[9] and in[10] correspond precisely to the one found by Williams[11] for plane strain, i.e. as if $R_0 \to \infty$ in Fig. 1. The implication of course is that, as $\rho \to 0$, the condition is one of plane strain; it makes no difference whether tractions vanish at $\phi = 0$ and clamping is at $\phi = \pi/2$, or vice versa. While the arguments for this result are convincing, the implications for engineering use of the result are not always fully understood; there is some need to know the stress field in the vicinity of the corner as well as at its precise position.

In this paper we discuss a sequence of cylinder problems, analyzed via a special finite element method which resolves considerable detail of the stress field in the vicinity of the corner. The method is a particular, i.e. axisymmetric, case of a general approach described earlier[12]. It is designed to elicit the strength of the singularity and to provide a detailed database with respect to the stress field which may be examined by itself or which may be used to extract an appropriate measure of local stress intensity. Moreover, the method is adaptable immediately to other shapes, e.g. V-notches or re-entrant corners. The problems reported here include two long cylinders, one solid and one hollow, with clamped ends; a long cylinder with its outer diameter constrained; and a thin disk whose faces are clamped. In general, our findings are not at variance with those in the literature, but our results do provide further insight into these problems and thereby form a useful supplement to prior work.

METHOD OF SOLUTION

In Fig. 2, we show the placement of a typical special element at the vertex of the singular region. As indicated, the element has five nodes and it occupies the space $0 < \rho < 2\rho_e$, $\phi_1 < \phi < \phi_2$ in the local toroidal coordinates. An array of these elements models the vertex $\phi_a < \phi < \phi_b$; this array is then embedded in a host field of "regular" finite elements—here, linear displacement, three node, axisymmetric triangles[13]. Note that Fig. 2 is drawn for any corner in the (r, z) frame and individual cases are defined by adjusting ϕ_a and ϕ_b.

We proceed under the assumption that the behavior of the stress field near the vertex $(\rho \to 0)$ is dominated by a singularity whose form is

$$c\rho^{q-1}, \quad (0 < q < 1) \tag{1}$$

where c is a measure of the stress intensity and q indicates the strength of the singularity. In addition to the displacements which correspond to (1), the stiffness approach of the finite element method requires displacement fields that permit rigid body motion as well as constant strains. Accordingly, the following global (r, z) displacement components are assumed to take the form

$$\begin{aligned} u &= u_0 + Ar + Cz + (E + F\phi)\rho^q \cos\phi - (G + H\phi)\rho^q \sin\phi \\ w &= w_0 + Bz + Dr + (E + F\phi)\rho^q \sin\phi + (G + H\phi)\rho^q \cos\phi. \end{aligned} \tag{2a}$$

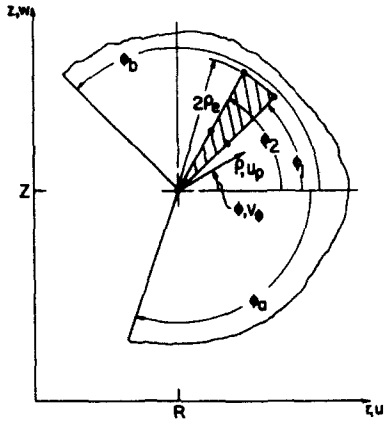

Fig. 2. A five node special element.

The corresponding components in the local coordinate frame are

$$\begin{aligned} u_\rho &= A\rho\cos^2\phi + B\rho\sin^2\phi + (C+D)\rho\sin\phi\cos\phi + (E+F\phi)\rho^q + (u_0 + AR + CZ)\cos\phi \\ &\quad + (w_0 + DR + BZ)\sin\phi \\ v_\phi &= D\rho\cos^2\phi - C\rho\sin^2\phi + (B-A)\rho\sin\phi\cos\phi + (G+H\phi)\rho^q + (w_0 + DR + BZ)\cos\phi \\ &\quad - (u_0 + AR + CZ)\sin\phi. \end{aligned} \tag{2b}$$

Note that the displacement behavior corresponding to (1) also allows for linear variation in the circumferential direction via the fourth terms in each of (2b). The coefficients $A,B,_{,,,}$ are then eliminated from (2) to obtain displacements in terms of nodal values of ρ and ϕ. After some algebra, we have

$$\{u\} \equiv \{u\ w\}^T = [\alpha(\rho, \phi; q)]\{\hat{u}\} \tag{3}$$

in which the components of $[\alpha]$ are the interpolation functions and $\{\hat{u}\}$ represents a vector of nodal displacements. For any particular element

$$\{\hat{u}\}^T = \{u_1\ w_1 \ldots u_5\ w_5\}.$$

Differentiation of (3) gives the strains in axisymmetric elasticity as

$$\{\epsilon\} \equiv \{\epsilon_r \epsilon_z \gamma_{rz} \epsilon_\theta\}^T = [\beta(\rho, \phi; q)]\{\hat{u}\} \tag{4}$$

where $[\beta]$ is termed the strain matrix. We also define the elasticity matrix by

$$\{\sigma\} \equiv \{\sigma_r \sigma_z \tau_{rz} \sigma_\theta\}^T = [D]\{\epsilon\}. \tag{5}$$

The potential energy of an individual special element of volume V_s is of the form

$$\Pi^s = \frac{1}{2}\int_{V_s} \{\sigma\}^T\{\epsilon\}\,\mathrm{d}V - \int_{S_\sigma} \{u\}^T\{t\}\,\mathrm{d}S \tag{6}$$

in which $\{t\}$ is the vector of tractions prescribed on the appropriate portion S_σ of the element's area (for simplicity we have omitted initial strains and body forces). Noting that $\mathrm{d}V = 2\pi(R + \rho\cos\phi)\rho\,\mathrm{d}\phi\,\mathrm{d}\rho$ and combining (3), (4) and (5) with (6) results in

$$\Pi^s = \pi\{\hat{u}\}^T \int_{\phi_1}^{\phi_2}\int_0^{2\rho_e} [\beta]^T[D][\beta](R + \rho\cos\phi)\rho\,\mathrm{d}\rho\,\mathrm{d}\phi\{\hat{u}\} - \{\hat{u}\}^T \int_{S_\sigma} [\alpha]^T\{t\}\,\mathrm{d}S.$$

We regard the functional Π^s as being dependent upon $\{\hat{u}\}$ and the exponent q; hence, it provides the special aspect of this element.

Equating the first variation of Π^s with zero, we have

$$\delta\Pi^s = \frac{\partial\Pi^s}{\partial\{\hat{u}\}}\delta\{\hat{u}\} + \frac{\partial\Pi^s}{\partial q}\delta q = 0. \tag{7}$$

A moment's reflection shows that a null value of the first term on the right of (7) is equivalent to the familiar elemental stiffness equation relating nodal forces $\{F_s\}$ to $\{\hat{u}\}$

$$[K_s]\{\hat{u}\} = \{F_s\} \tag{8}$$

where

$$\begin{aligned} [K_s] &= 2\pi\int_{\phi_1}^{\phi_2}\int_0^{2\rho_e} [\beta]^T[D][\beta](R + \rho\cos\phi)\rho\,\mathrm{d}\rho\,\mathrm{d}\phi \\ \{F_s\} &= \int_{S_\sigma} [\alpha]^T\{t\}\,\mathrm{d}S. \end{aligned} \tag{8a}$$

The integrals in (8a) are complex and are computed numerically by Gauss quadrature using seven radial and three angular sampling positions.

The second term in (7) represents the variation of the potential energy with respect to the singular exponent. Clearly, this may lead to a different value of q for each special element. However, we take q to be the same for all the elements, in agreement with what we know of such singular behavior[11]; i.e. that the singularity is independent of spatial coordinates. As we will show below, q should be calculated and potential energy minimized on a global basis. Moreover, to permit q to vary from one element to the next would introduce a discontinuity of displacements between adjacent special elements.†

We now turn our attention to the global analysis. The total potential energy of the complete structure, consisting of n special elements and m regular elements is simply

$$\Pi^t = \sum_{i=1}^{n} \Pi_i^s + \sum_{i=1}^{m} \Pi_i^r$$

where the superscript r denotes regular elements. Taking the same strategy in the global analysis and noting that Π_i^r is independent of q, yields

$$\delta\Pi^t = \frac{\partial \Pi^t}{\partial \{a\}} \delta\{a\} + \frac{\partial}{\partial q} \sum_{i=1}^{n} \Pi_i^s \delta q = 0 \tag{9}$$

where $\{a\}$ is a vector containing all of the nodal degrees of freedom of the structure. Hence, the result (9) of minimizing the functional Π^t with respect to all nodal displacements $\{a\}$ and q is the following simultaneous conditions

$$[K]\{a\} = \{F\} \tag{10a}$$

$$\sum_{i=1}^{n} \Pi_i^s = \text{minimum with respect to } q \tag{10b}$$

where $[K]$ is the assembled global stiffness matrix and $\{F\}$ is a vector of prescribed nodal forces. Note that by (10b) q is tacitly required to be the same for the complete sector of special elements.

The solution algorithm begins by solving (10a) for any value of q within the range specified by (1). The potential energy is calculated and minimized by adjusting q such that (10b) is satisfied. Using the new value of q, the global stiffness equation is solved again. This procedure is repeated until (9) is satisfied to some appropriate numerical precision.

The formulations described above are incorporated in a finite element computer code called AXISPL[16]. For the problems treated with this code, storage requirements on a DEC 2060 are approximately 50,000 words, including some double precision usage necessitated by the size of R_0 relative to ρ_c.

ANALYSIS AND RESULTS

Four circular cylinders were chosen for analysis. Three of the cylinders have stress free curved surfaces and constrained ends. These include a long solid cylinder, a long hollow cylinder, and a thin solid disk. The remaining problem is a long solid cylinder with stress free ends and a constrained curved surface; the outer diameter is displaced radially but not axially. As shown in Fig. 3, the long cylinders were analyzed with the same finite element map, with the following proportions, long solid cylinder: $L/D = 2.5$, $R_i/R_0 = 0$; long hollow cylinder: $L/D = 1.25$, $R_i/R_0 = 0.5$. This map has 414 degrees of freedom. No attempt was made to capture the singularity at R_i; its highly localized nature should not affect behavior at R_0. We thus have the advantage of comparing results from a single map under different loadings.

†There remains, however, an interelement incompatibility at the interface ($\rho = 2\rho_c$) of the special and regular elements. Based on the patch test, on previous work[12, 14, 16], and the results reported herein, this difficulty is negligible.

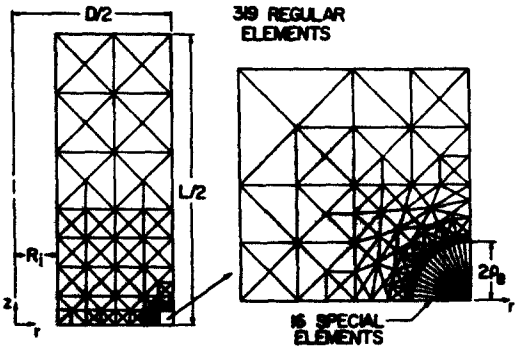

Fig. 3. Axisymmetric finite element model used in the analysis of the long circular cylinders.

The thin disk† was modeled as shown in Fig. 4. It has 316 degrees of freedom and the following proportions, $L/D = 0.0625$, $R_i/R_0 = 0$.

The nodal boundary and symmetry conditions for the long solid cylinder and thin disk with constrained ends are

$$\begin{aligned} r = R_0; &\quad \sigma_r = 0, &\quad \tau_{rz} = 0 \\ r = 0; &\quad u = 0, &\quad \tau_{rz} = 0 \\ z = 0; &\quad u = 0, &\quad w = 0 \\ z = L/2; &\quad w = w_0, &\quad \tau_{rz} = 0 \end{aligned}$$

in which w_0 is a constant. For the long hollow cylinder, the second of the above is replaced with

$$r = R_i; \quad \sigma_r = 0, \quad \tau_{rz} = 0.$$

For the long solid cylinder with the curved surface constrained, the imposed nodal conditions are

$$\begin{aligned} r = R_0; &\quad u = u_0, &\quad w = 0 \\ r = 0; &\quad u = 0, &\quad \tau_{rz} = 0 \\ z = 0; &\quad \sigma_z = 0, &\quad \tau_{rz} = 0 \\ z = L/2; &\quad w = 0, &\quad \tau_{rz} = 0 \end{aligned}$$

where u_0 is a constant.

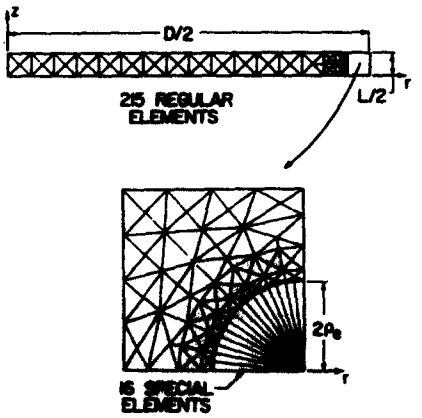

Fig. 4. Axisymmetric finite element model used in the analysis of the thin disk.

†A thin clamped disk under simple extension is sometimes referred to as the poker chip problem[15].

Each of the four cylindrical configurations was analyzed assuming a linear elastic, homogeneous, isotropic material with Young's modulus and values of Poisson's ratio as

$$E = 25 \times 10^6 \text{ psi}$$

$$\nu = 0.20, 0.25, 0.30.$$

CPU time for these analyses was approximately 30 seconds per iteration on a DEC 2060 and, typically, two to four iterations were required.

We now turn our attention to the computation of the singularity exponent q. As previously mentioned, the works of both Zak[9] and Benthem and Minderhoud[10] show that the eigenfunction in the vicinity of the singularity is identical to the form derived by Williams[11] for a clamped-free wedge of angle η, namely

$$\sin^2 \lambda\eta = \left[\frac{4(1-\nu)^2}{3-4\nu}\right] - \left[\frac{\sin^2 \eta}{(3-4\nu)\eta^2}\right]. \tag{11}$$

The eigenvalue λ is defined through its use in

$$\chi(\rho, \phi) = \rho^{\lambda+1} F(\phi; \lambda)$$

in which χ is the Airy stress function and is a biharmonic function in polar coordinates. It is a simple matter to show that in the range $0 < \lambda < 1$, strains and stresses are singular. Clearly, the exponent q used in this paper is equivalent to the lowest real positive root (λ_1) of (11). Computed values of q vs ν are plotted in Fig. 5, along with λ_1 as derived from (11). It is evident that the overall behavior of λ_1 and q vs ν is the same, although there is a definite shift in magnitudes for the long cylinders.

The differences between λ_1 and q may be due to modeling sources, two of which are obvious. The special elements, after all, are finite: Figs. 3 and 4 show $2\rho_e/(R_0 - R_i) = 1/32$ for the cylinders. To maintain numerical precision, finiteness is required, whereas the eigenanalysis is for the limiting case, $\rho \to 0$. Prior studies[14, 16] have shown minimal sensitivity of the exponent to the radial size of the special element, with the trend in the proper direction. All evidence in hand thus points to $q \to \lambda_1$ precisely as $\rho_e \to 0$ but, unfortunately, this is a limit we cannot test.

A more important source of difference between q and λ_1 is what may be termed eigenvalue smearing. Recall from (1) and the subsequent element formulation that we model behavior of strain and stress as

$$c_1 \rho^{q-1} + c_2 \tag{12}$$

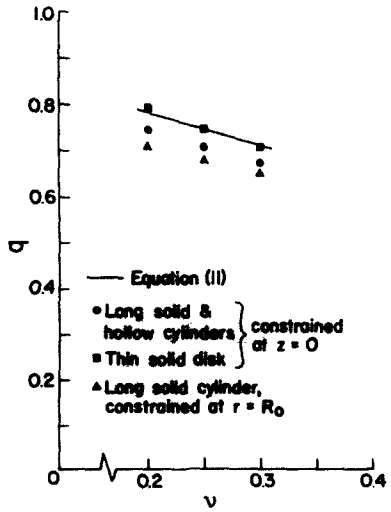

Fig. 5. Singularity exponent q vs Poisson's ratio for each cylinder problem.

On the other hand, (11) has an infinity of roots, the lowest of which is real and in the open interval 0, 1. Beyond that, Zak[9] tabulates the next 19 roots as complex. To represent the formal eigenanalysis, the expression (12) must be adjusted to a slightly different form:

$$\bar{c}_1\rho^{\lambda_1-1}+\bar{c}_2\rho^{\lambda_2-2}+\ldots$$

The result is that the coefficients in (2) will be affected; in addition the exponent q may reflect some difference. To test the magnitude of this effect, the present element would require reformulation with seven nodes, the introduction of a second special term having an exponent p, and minimization as in (10b) with respect to both exponents, each operating in its own interval. We believe the quality of the present results does not warrant such an extension of the model.

Angular variations of stress components are shown in Figs. 6–9 for one local radial position and one value of Poisson's ratio. For the cylinders with constrained ends, all stress components are normalized by the resultant axial stress and for the one cylinder with the constrained radial surface we use the resultant radial stress. These values are computed from discrete nodal reaction forces (10a) in the finite element analysis, as opposed to element values of the respective stress components.

Notice that the high stress gradients are smoothly depicted. The major difference between the results for each cylinder is the amplitude of the stresses. The overall differences are better compared by plots of principal stresses, maximum shear stress and strain energy density, as illustrated in Figs. 10–12, respectively. Also, note that the expected symmetry between constrained plane ends and constrained curved surface solid cylinders is readily apparent, although there is a slight difference in amplitude. For all the cylinders, it is evident that the maximum shear stress and strain energy density peak in the range of 25–35 deg, measured from the free surface. Radial distributions of some of the same quantities appear in Figs. 13–15. Computed stress σ_z and τ_{rz} from the long solid cylinder analysis are in good agreement with those reported by Benthem and Minderhoud[10] for a semi-infinite cylinder.

Apparently, stress is affected by changing values of R_i/R_0 and L/D, whereas the singular behavior of the stress is relatively unaffected by these same quantities. This dependence of the intensity of stress on curvature is coincidentally in agreement with the numerical results reported by Swedlow and Ritter[17], for cracked cylinders in simple tension.

CONCLUSIONS

In this paper we demonstrate that a special finite element method can be a satisfactory tool for determining the stress distribution in axisymmetric structures containing singularities. The method indicates both the intensity and nature of singularity via a simple minimum potential

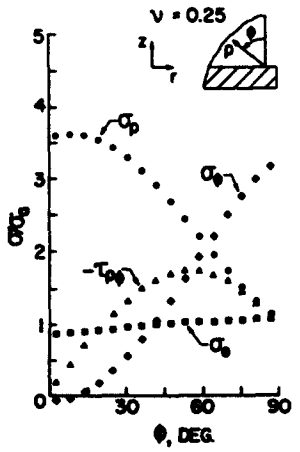

Fig. 6.

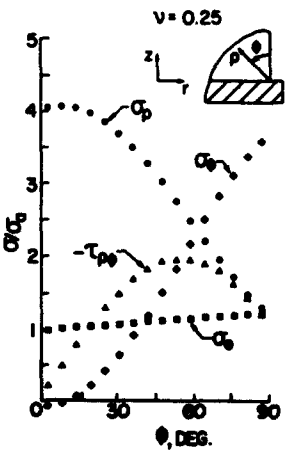

Fig. 7.

Fig. 6. Angular variation of σ/σ_a at $\rho/(R_0-R_i)\sim 0.0008$ for the long solid cylinder with constrained ends.

Fig. 7. Angular variation of σ/σ_a at $\rho/(R_0-R_i)\sim 0.0008$ for the long hollow cylinder with constrained ends.

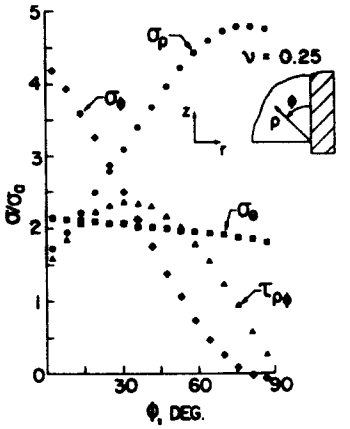

Fig. 8.

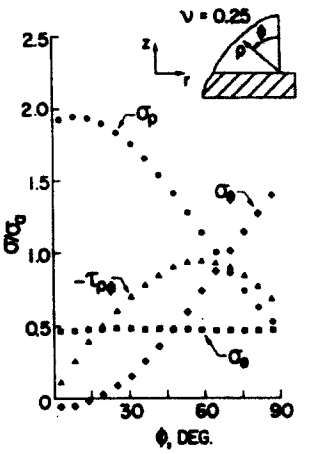

Fig. 9.

Fig. 8. Angular variation of σ/σ_a at $\rho/(R_0 - R_i) \sim 0.0008$ for the long solid cylinder with constrained curved surface.

Fig. 9. Angular variation of σ/σ_a at $\rho/(R_0 - R_i) \sim 0.0008$ for the thin disk with constrained ends.

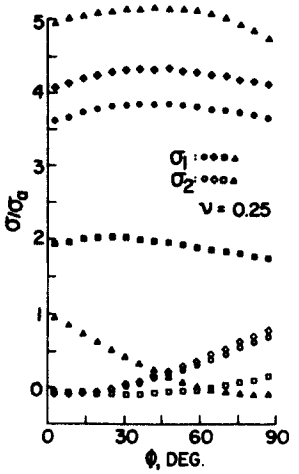

Fig. 10.

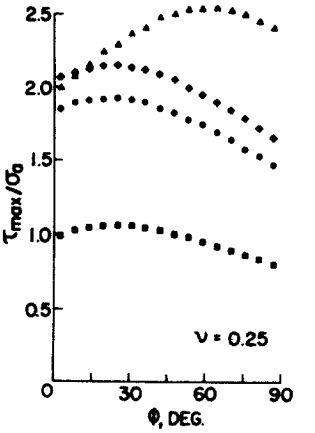

Fig. 11.

Fig. 10. Angular variation of σ/σ_a at $\rho/(R_0 - R_i) \sim 0.0008$. Legend per Fig. 5, except diamonds represent the hollow cylinder.

Fig. 11. Angular variation of τ_{max}/σ_a at $\rho/(R_0 - R_i) \sim 0.0008$.

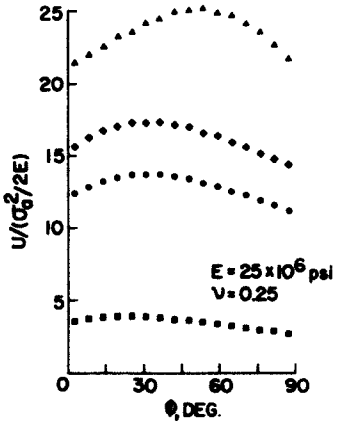

Fig. 12.

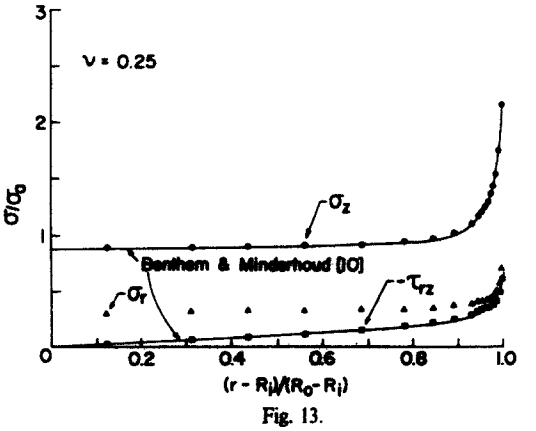

Fig. 13.

Fig. 12. Angular variation of $U/(\sigma_a^2/2E)$ at $\rho/(R_0 - R_i) \sim 0.0008$.

Fig. 13. Radial variation of σ/σ_a at $z = 0$ for the long solid cylinder with constrained ends.

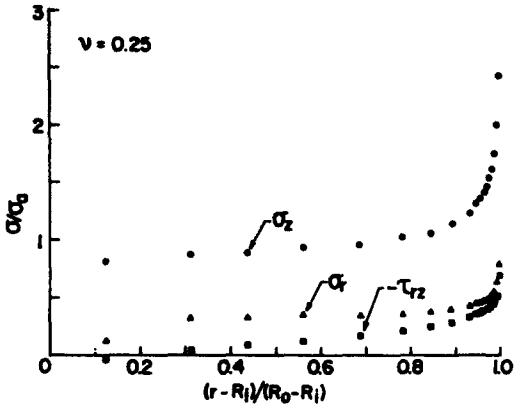

Fig. 14. Radial variation of σ/σ_a at $z = 0$ for the long hollow cylinder with constrained ends.

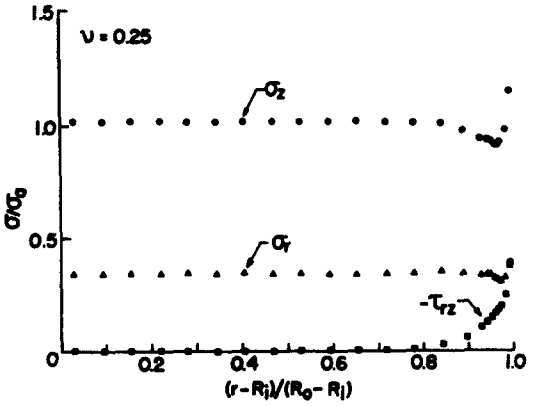

Fig. 15. Radial variation of σ/σ_a at $z = 0$ for the thin solid disk with constrained ends.

energy technique. For the constrained cylinders analyzed, the singular behavior is relatively unaffected by curvature and length. The intensity of the stress field is, however, dependent upon these quantities. While the range of applicability has been limited to right circular cylinders, the method can be applied to other problems where the singularities are not well known. Such problems would involve further geometric complexity as encountered in engineering practice, a wider range of load configuration and constraint and material anisotropy. That the method may be extended to incorporate elasto-plastic flow is evident as well[14].

Acknowledgement—The work reported above was sponsored by the Department of the Navy, Office of Naval Research through Grant No. N00014-78-C-0528. The authors are sincerely grateful for their support.

REFERENCES

1. L. N. G. Filon, On the elastic equilibrium of circular cylinders under certain practical systems of load. *Phil. Trans R. Soc. (Lond.)* A198, 147–233 (1902).
2. G. Pickett, Application of the Fourier method to the solution of certain boundary problems in the theory of elasticity. *J. Appl. Mech.* 66, A176–A182 (1944).
3. G. Horvay and J. A. Mirabal, The end problem of cylinders. *J. Appl. Mech.* 25, 561–570 (1958).
4. A. Mendelson and E. Roberts, Jr., The axisymmetric stress distribution in finite cylinders. In *Developments in Mechanics*, Vol. 2, Part 2 pp. 40–57, Proceedings of the 8th Midwestern Mechanics Conference. Pergamon Press, Oxford (1963).
5. H. Kaehler, Stress analysis of finite length cylinders by station functions. *AIAA J.* 3, 2132–2137 (1965).
6. R. W. Little, Elastostatic boundary region problem in solid cylinders. *Quart. Appl. Math.* 25, 261–274 (1967).
7. W. E. Warren, A. L. Roark and W. B. Bickford, End effect in semi-infinite transversely isotropic cylinders. *AIAA J.* 5, 1448–1455 (1967).
8. G. W. Swan, The semi-infinite cylinder with prescribed end displacements. *SIAM J. Appl. Math.* 16, 860–881 (1968).
9. A. R. Zak, Elastic analysis of cylindrical configurations with stress singularities. *J. Appl. Mech.* 39, 501–506 (1972).
10. J. P. Benthem and P. Minderhoud, The problem of the solid cylinder compressed between rough rigid stamps. *Int. J. Solids Structures* 8, 1027–1042 (1972).
11. M. L. Williams, Stress singularities resulting from various boundary conditions in angular corners of plates in extension. *J. Appl. Mech.* 19, 526–530 (1952).

12. J. L. Swedlow, Singularity computations. *Int. J. Numerical Methods in Engng* 12, 1779–1798 (1978).
13. R. H. Gallagher, *Finite Element Analysis Fundamentals*, pp. 311–316. Prentice-Hall, Englewood Cliffs, New Jersey (1975).
14. M. E. Karabin, Jr., Elastic–plastic flow in cracked bodies using a new finite element model. Ph.D. Thesis. Department of Mechanical Engineering, Carnegie-Mellon University (1977).
15. G. H. Lindsey, R. A. Schapery, M. L. Williams and A. R. Zak, The triaxial tension failure of viscoelastic materials. ARL 63-152, California Institute of Technology (1963).
16. J. S. Solecki, Unpublished research (1978–79).
17. J. L. Swedlow and M. A. Ritter, Toward assessing the effects of crack front curvature (CFC). *Stress Analysis and Growth of Cracks*, pp. 79–89, STP 513. ASTM, Philadelphia (1972).